Fluorescence double resonance optical pumping spectrum and its application for frequency stabilization in millimeter scale vapor cells

Journal of Physics Communications

OPEN ACCESS

RECEIVED
6 September 2017

REVISED
26 September 2017

ACCEPTED FOR PUBLICATION
16 October 2017

PUBLISHED
20 December 2017

PAPER

Fluorescence double resonance optical pumping spectrum and its application for frequency stabilization in millimeter scale vapor cells

Eliran Talker, Liron Stern, Alex Naiman, Yefim Barash and Uriel Levy

Department of Applied Physics, The Benin School of Engineering and Computer Science, The Center for Nanoscience and Nanotechnology, The Hebrew University of Jerusalem, Jerusalem, 91904, Israel

E-mail: ulevy@mail.huji.ac.il

Keywords: atomic spectra, laser frequency stabilization, absorption spectroscopy, fluorescence spectroscopy, atomic excitation

Abstract

In recent years, we are observing substantial efforts towards the miniaturization of atomic cells to a millimeter scale and below, with the ultimate goal of enabling efficient and compact light vapor interactions. However, such miniaturization results in a reduction in optical path, effectively reducing the contrast of the optical signal. In order to overcome this obstacle, we have introduced and demonstrated a new approach of fluorescence double resonance optical pumping (FDROP) in the ladder-type atomic system. We have developed a theoretical model to predict the FDROP spectrum and validated this model using experimental results in a millimeter-size cell. We show that the contrast of fluorescence signal of the FDROP approach is higher than the transmission signal in the double resonance optical pumping approach. Taking advantage of this desired property, we have used the FDROP for the purpose of stabilizing the frequency of a laser operating at the telecom waveband with the hyperfine structure of the $5P_{3/2}$–$4D_{5/2}$ transition in a millimeter-size cell. By beating the stabilized laser to another stabilized laser, we obtained frequency instability floor of 9×10^{-10} at around 1000 s in terms of Allan deviation. Such sources which are stabilized to miniaturized cells may play an important building block in diverse fields ranging e.g. from communication to metrology.

1. Introduction

Laser spectroscopy employing miniaturized vapor cells is attracting growing attention, primarily for its potential applications in compact frequency standards [1–3], laser cooling [4–7], magnetometry [8–10] and optical isolation [11], to name a few. In order to obtain a highly resolved spectral lines in the transition from one excited state to another, various optical pumping methods, such as the optical-optical double resonance (OODR) technique, have been successfully used [12].

Recently, Moon *et al* used the double resonance optical pumping (DROP) technique to observe a well-resolved spectral lines with a high signal-to-noise ratio (SNR) in the transition between excited states [13]. Basically, the DROP spectrum is obtained by optical pumping from one of the hyperfine levels of the ground state to another hyperfine level through the excited state and the intermediate states in the ladder-type atomic system [2]. In spite of the fact that DROP offers a high SNR as compared to OODR, the results demonstrated so far were based on vapor spectroscopy in relatively large (centimeter scale) cells. In fact, in a miniaturized cell (mm size scale and below) it is still very challenging to observe DROP signal, because the DROP signal, being based on absorption, is masked by a strong background. This is in contrast to the fluorescence signal, which potentially offers lower background level.

Herby, we take advantage of this property of the fluorescence signal and introduce for the first time a spectroscopic method which we coin 'fluorescence double resonance optical pumping (FDROP)'. We show theoretically and experimentally that our FDROP approach can improve the contrast of the signal with respect to the DROP approach and thus can be used for laser spectroscopy in miniaturized cells. The comparison between FDROP and DROP is performed for different coupling laser's power within a millimeter-size cell. The

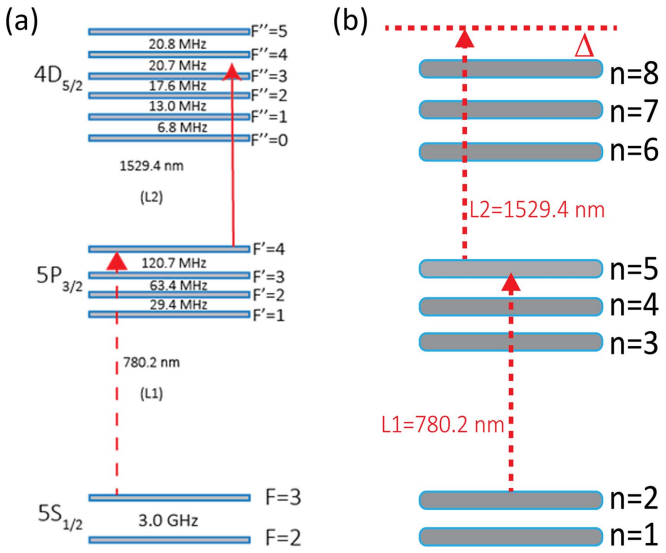

Figure 1. Energy level diagram for FDROP and DROP, (a) real level diagram for ^{85}Rb. (b) Eight level diagram used for the theoretical model.

obtained experimental results emphasis the advantages of the FDROP approach over large range of intensities. Following, we utilize this approach for demonstrating frequency stabilization of a laser diode to the hyperfine structure of the $4D_{5/2}$ transition in a mm size cell.

2. Theory

The theory of the FDROP approach is based on the interaction of atoms with two optical fields that are resonantly tuned to two transitions that share a common state. Essentially, the FDROP simply detects the change in population of the intermediate state ($F' = 2, 3, 4$, figure 1). When the atoms are resonant with the fields of the two lasers L1 and L2, the population of the intermediate state is depleted. By detecting this population, we observe a dip in the fluorescence signal. Figure 1(a) shows the relevant energy levels of rubidium atoms. The center wavelengths of the transitions of $5S_{1/2}$–$5P_{3/2}$ and $5P_{3/2}$–$4D_{5/2}$ are 780.2 nm and 1529.4 nm, respectively. The spontaneous decay rate from $5P_{3/2}$ to $5S_{1/2}$ state is $\Gamma_1 = 2\pi \times 6.06$ MHz [14], and that of the $4D_{5/2}$ to $5P_{3/2}$ is $\Gamma_2 = 2\pi \times 1.97$ MHz [15]. The probe laser (L1) is assumed to be locked to the $F = 3$ to $F' = 4$ cycling transition, while the coupling laser (L2) is scanned over the entire range of the excited states in the $4D_{5/2}$ transitions. The FDROP spectrum is calculated by probing the fluorescence of the $4D_{5/2}$ states as a function of the laser frequency for various powers of the coupling beam. Our model assumes an eight-level ladder-type atomic system as shown in figure 1(b) and use the Einstein rate equations in order to calculate the steady state population densities.

The signal is assumed to be measured over large time scales such that oscillations generated by coherent effects can be neglected. The model also assumes collimated pump and probe beams, with spectral widths smaller than the spontaneous decays rates of the atoms. The FDROP signal, apart from a proportionality factor, can be calculated by integrating the $N_{F'}$ (i.e. the intermediate population density) over the thermal velocity distribution and summing over all the intermediate states i.e.

$$I_{\mathrm{flu}}(\Delta) \propto \sum_{F'} \int_{-\infty}^{\infty} N_{F'}(\Delta, v) \cdot W(v)\mathrm{d}v,$$

where $W(v)$ is the one dimensional Maxwellian velocity distribution, which is given as

$$W(v) = \frac{1}{\sqrt{\pi u_p}} \exp\left(-\frac{v^2}{u_p^2}\right),$$

where $u_p = \left(\frac{2k_{\mathrm{B}}T}{m}\right)^{\frac{1}{2}}$ is the most probable velocity, k_{B} is the Boltzmann's constant, m is the mass of the atom, and T is the temperature in Kelvin. As mentioned, the population is found using rate equations (see appendix for more details).

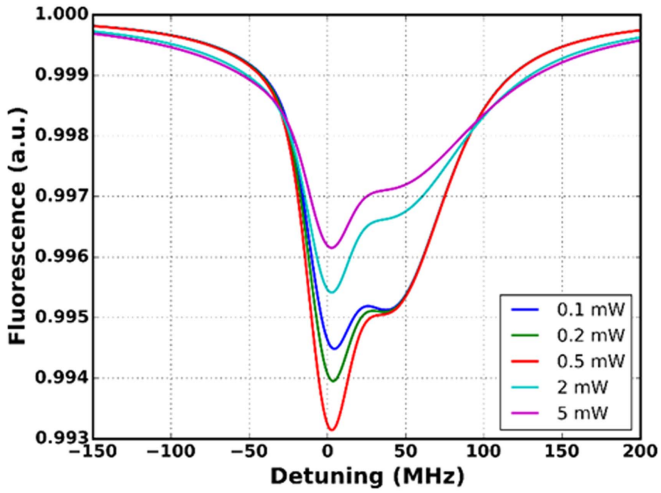

Figure 2. Calculated FDROP spectrum at different coupling laser power for the transitions $5S_{1/2}$–$5P_{3/2}$–$4D_{5/2}$.

Figure 2 shows the calculated spectrum of the FDROP signal for the transition $5S_{1/2}$–$5P_{3/2}$–$4D_{5/2}$ for several values of coupling laser power. The power of the probe laser and the temperature were set to 15 mW and 70 °C, respectively for used cell of length 1 mm. From figure 2, we can see that the contrast of the signal is strongly dependent on the coupling laser power. At first, the contrast is improving with the increase in coupling laser power. This is expected, as the growth in photon flux excites more atoms from the intermediate state (F') to the excited state (F''). However, further increase in coupling power results in a decrease in the contrast of the signal. This is because as the coupling power continues to increase, the rate of optical pumping increases as well, resulting in the depletion of the intermediate F' levels. We therefore expect that the FDROP approach will be attractive in particular for low light applications, e.g. few photon switching. We further note that the line width of the signal is also increasing with the power of the coupling laser beam. Indeed, the line width of the FDROP spectrum in mm scale cell is affected mainly by power broadening.

3. Experimental setup

Next, we turn into the demonstration of the measured results. The experimental setup for detecting the fluorescence and the transmission is described in very similar to the setup originally introduced by Moon *et al* [13]. In short, two laser beams, the probe laser and coupling laser, are counter-propagating through an Rb vapor cell. The transmission of the L1 laser is measured in order to obtain the DROP spectra whereas the fluorescence from the $5P_{3/2}$ levels is collected as the FDROP spectra. The schematic for experimental setup and the photograph of used mm size Rb cell is shown in figures 3(a), (b) respectively.

As was previously indicated (figure 1(a), red dashed lines), the probe beam (L1) is fixed on the cyclic $5S_{1/2}$–$5P_{3/2}$ transition of the ^{85}Rb D2 line. This is obtained using a conventional frequency modulation technique for saturated absorption spectroscopy (SAS) [5, 18]. The wavelength of the L1 laser is around 780 nm and that of the lasers L2, and L3 is around 1529 nm respectively. We lock the frequency of the L1 laser to the $5S_{1/2}$ ($F = 3$) to $5P_{3/2}$ ($F' = 4$) transition in the ^{85}Rb D2 line. The frequency of the L2 and L3 lasers around 1529 nm can be scanned over the entire range of excited states in the $5P_{3/2}$ to $4D_{5/2}$ transition. We control each of the laser's power by changing the diode current. We then direct the beams through an aperture of ~2 mm diameter through a 7.5 cm long Rb vapor cell (reference cell), and in parallel through a ~1 mm long miniaturized Rb vapor cell. The fluorescence and the transmission signals are detected by a Si photodiode.

4. Experimental results

We start by presenting a snapshot of the experimental results, providing a comparison between the FDROP and the DROP signal collected from a miniaturized (mm scale) Rubidium (Rb) hot vapor cell. The DROP spectrum is captured by measuring the transmission of the laser while the FDROP spectrum is captured by measuring the fluorescence from the $5P_{3/2}$ levels. Typical results are shown in figure 4.

As can be seen, under the operation conditions reported above, the DROP signal cannot be observed while the FDROP transition is easily traceable. This is mainly due to the fact that the DROP spectrum is masked by the

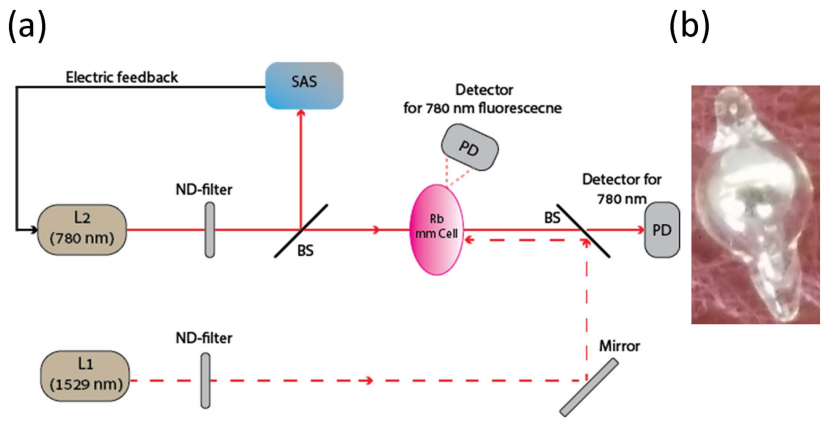

Figure 3. (a) Schematic drawing of the experimental setup (BS: beam splitter; PD: photo-diode; SAS: saturated absorption spectroscopy) (b) image of the mm size Rb cell.

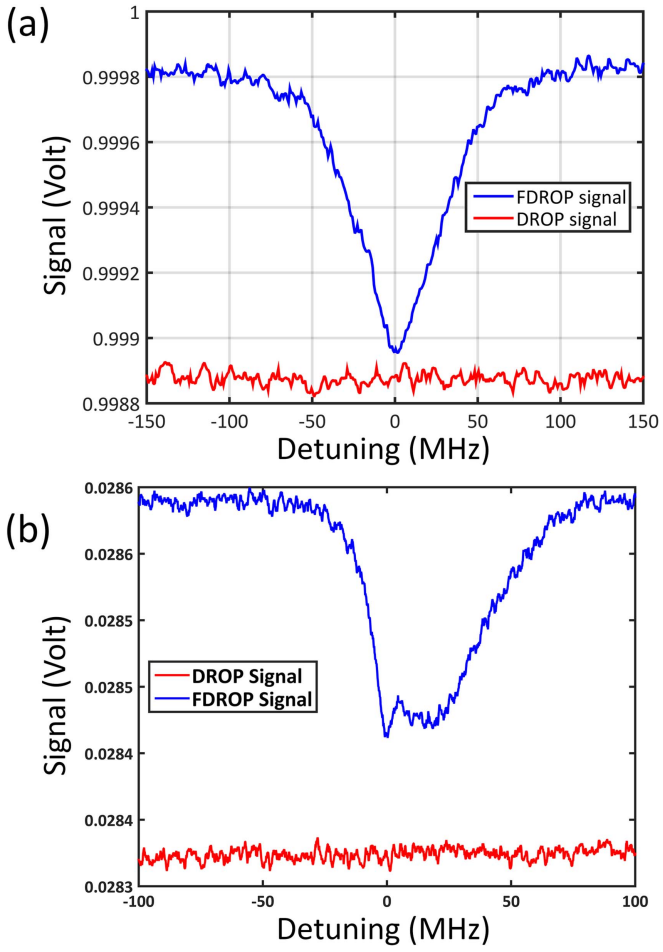

Figure 4. Comparison between FDROP and DROP signal; (a) FDROP and DROP spectrum at room temperature and coupling power of 5 mW; (b) FDROP and FDROP spectrum at 70 °C and coupling power of 50 μW.

strong transmission background coming from the probe laser. Indeed, it has been shown [6] that under conditions of low temperatures and coupling powers, the optical pumping efficiency is limited and therefore it is fairly challenging to observe the DROP spectra. In contrast, the FDROP signal is based on collecting the fluorescence which is not affected by the probe background. Another important factor which gives rise to the strong FDROP signal is the difference in lifetimes between the F'' levels and the F' levels. Due to the fact that the lifetime of the upper excited states ($F'' = 3, 4, 5$) is larger than the lifetime of the intermediate states ($F'' = 2, 3, 4$) by a factor of ~3 (84 ns and 27 ns, respectively), the F'' levels cannot be fully depleted to the F' levels, effectively

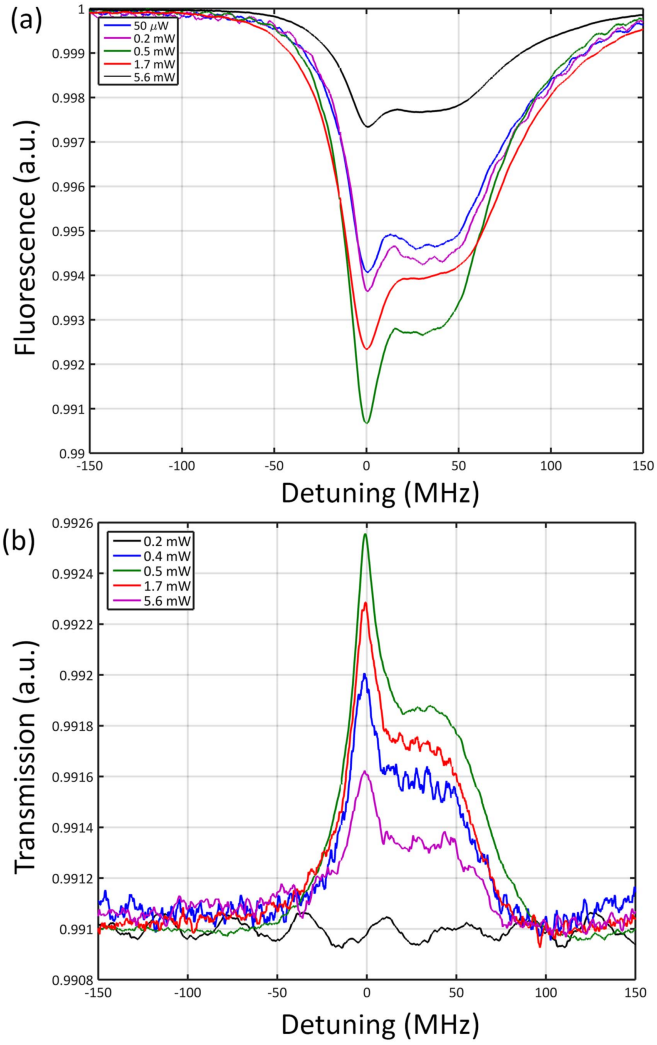

Figure 5. Experimental measurements of (a) FDROP spectra and (b) DROP spectra in mm scale cell as a function of the L2 laser's power in the $5P_{3/2}$–$4D_{5/2}$ transition of ^{85}Rb. All the measurements were performed under 70 °C. For comparison purposes, all curves in the FDROP signal are normalized to have the same contrast.

reducing the population of the F' levels. As a result, the strength of the fluorescence, i.e. the transition between the F' states to the ground states is reduced, which is shown as a dip in the fluorescence signal.

Next, we study the FDROP and DROP signal under various coupling powers. Figure 5(a), shows the FDROP spectrum obtained using the mm scale vapor cell at different coupling powers at a fixed temperature of 70 °C. In all cases, one can observe a clear signature of the fluorescence signal, even at a coupling power as low as 50 μW. As can be seen, the contrast of the signal is strongly dependent on the coupling power, similar to the modeling results presented above. Indeed, the contrast is first increasing with the coupling laser power, while further increase in power results in a contrast reduction. Additionally, we observe a slight broadening with the increase in coupling power, which is attributed to the effect of power broadening. This is also in line with the simulation results.

For comparison, we repeat the experiment at a similar temperature, this time measuring the transmission, i.e. collecting the DROP signal. As can be seen, higher coupling power (~0.4 mW) is needed in order to observe the signal. To further address the advantage of the FDROP approach over the DROP approach in spectroscopic measurements using mm size cells, we have extracted the transition contrast as a function of coupling power. The contrast, defined as $|S_H - S_L|/|S_H + S_L|$ where, $S_{H,L}$ stands for high and low signal, respectively, is plotted in figure 6 as a function of the coupling power.

As can be seen, the contrast of the FDROP signal is significantly higher than that of the DROP signal for a wide range of coupling powers. This serves as a good indication for the usefulness of the FDROP approach in vapor spectroscopy measurements with miniaturized cells. Furthermore, the plot shows explicitly the effect of contrast reduction for high coupling powers, as a result of the optical pumping effect.

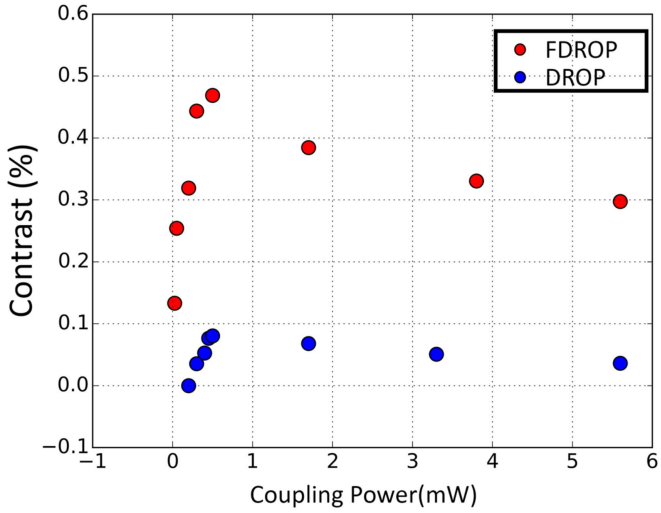

Figure 6. Contrast of the FDROP and DROP signal as a function of the coupling power at the wavelength of 1529 nm and constant temperature of 70 °C.

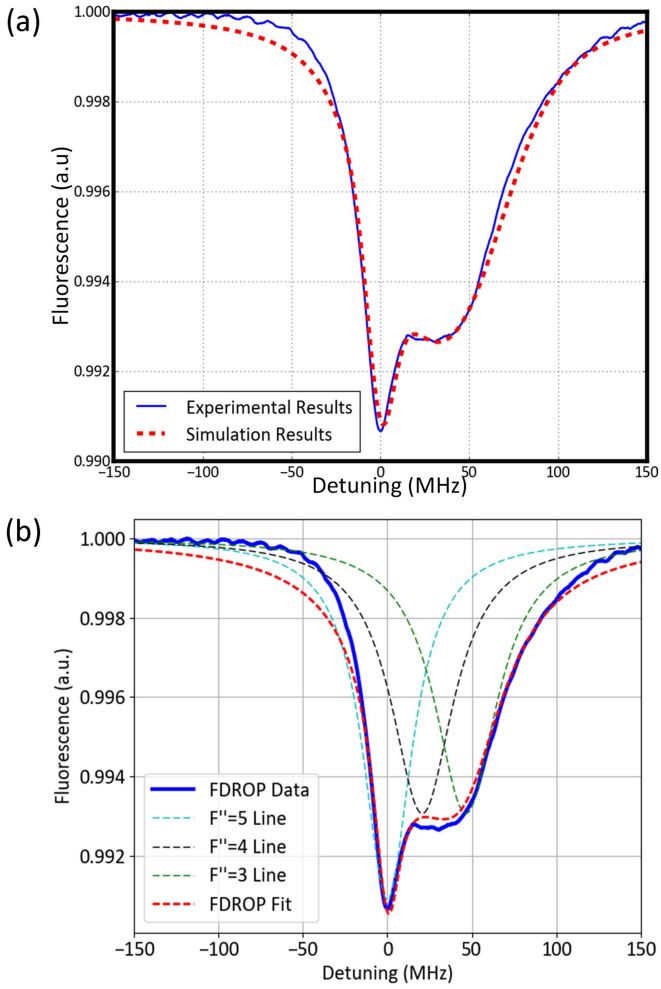

Figure 7. (a) Comparison between experimentally measured and calculated FDROP signal, under coupling laser power of 0.5 mW and temperature of 70 °C. Good agreement is obtained. (b) Curve fitting using three Lorentzians (shown by dashed cyan, green and black lines) for the results presented in figure 7(a). The red dashed line represents the sum of the three fitted Lorentzians.

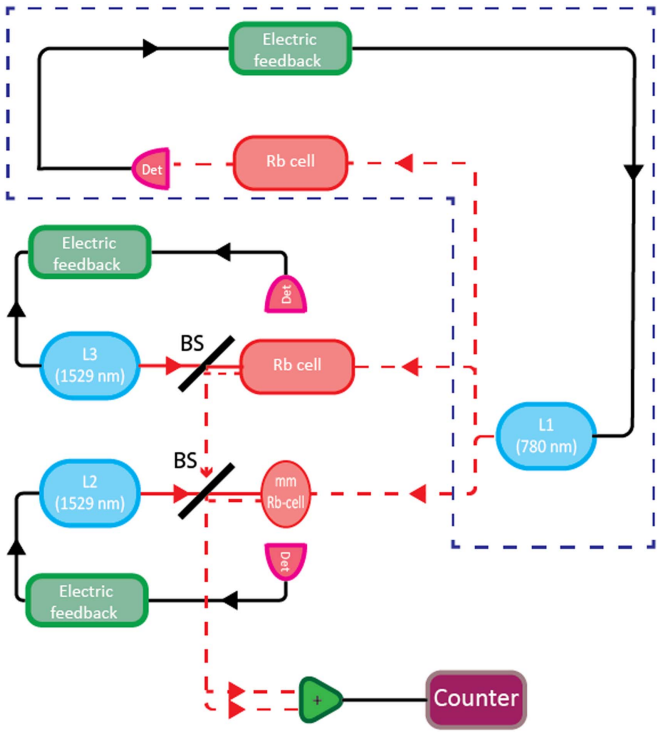

Figure 8. Frequency stabilization scheme; the loop surrounded by the blue dotted line is used to stabilize the 780 nm laser using SAS technique. The other loops are used to stabilize both the reference cell and the mm size cell. The dashed and the solid red lines are used for 780 and 1529 nm laser beams respectively. The black solid lines represent the electronic signals. (BS: beam splitter. Det: photo-diode).

For better comparison between the experimental results and the model, in figure 7(a), we present a comparison between the two, assuming a coupling power of 0.5 mW under temperature of 70 °C. One can observe a good agreement between the calculated and the experimental results. In figure 7(b), we show a fitting using three Lorentzian lines representing the transitions $F' = 4$ to $F'' = 3, 4, 5$, respectively. The line oscillator strength of each transition is taken from [13], and the FWHM of each Lorentzian, was found to be 50 MHz. As can be seen, the lines of the fitted Lorentzian are in overlap with one-another due to power broadening, and thus they cannot be easily resolved. The sum of the three Lorentzian fitting functions (dashed red line) was found to be in a good agreement with the obtained experimental result.

5. Laser stabilization with mm size cells by the aid of FDROP

In addition to spectroscopy, we take advantage of the superior contrast of the FDROP approach to demonstrate frequency stabilization in mm size cells at the telecom regime. The stabilization transfer scheme is presented in figure 8. As a reference, a tunable laser (L3) at telecom wavelength (HP 81682A) is stabilized to the $5P_{3/2}$ ($F' = 4$)–$4D_{5/2}(F'' = 4)$ transition, using a 7.5 cm reference cell which results in a narrow DROP line of ~6 MHz [16]. A similar tunable laser (L2) is locked to the mm size cell, using an FDROP signal. The level of instability is evaluated by beating the two tunable lasers at 1.5 μm (L2 and L3). The beat measurement is conducted with a fast photo detector (Agilent 11982A) followed by a high frequency counter (Agilent 53181A), having a frequency uncertainty floor level of 1 KHz, significantly beyond the precision needed for our experiment. In parallel, we lock a 780 nm laser (Toptica DL pro) to a standard Rb cell (7.5 cm long) using SAS technique.

It should be noted that the frequency of the L2 and L3 lasers was stabilized by electrically feeding back the error signal of the FDROP into the PZT of the two lasers, as shown in figure 8. We were able to obtain dispersion like error signal of the FDROP spectrum without extra frequency modulation for the L2 and L3 lasers by setting the phase sensitive detector of the lock-in amplifier according to the reference signal for the frequency modulation of the L1 laser. This was possible because the frequency of the L1 laser has already been modulated through SAS in order to stabilize the frequency of the laser. The scheme offers the advantage of obtaining the error signal of L2 and L3 lasers simply by modulating of the laser frequency of a single laser (L1), without directly modulating the frequency of the L2 and L3 lasers [16].

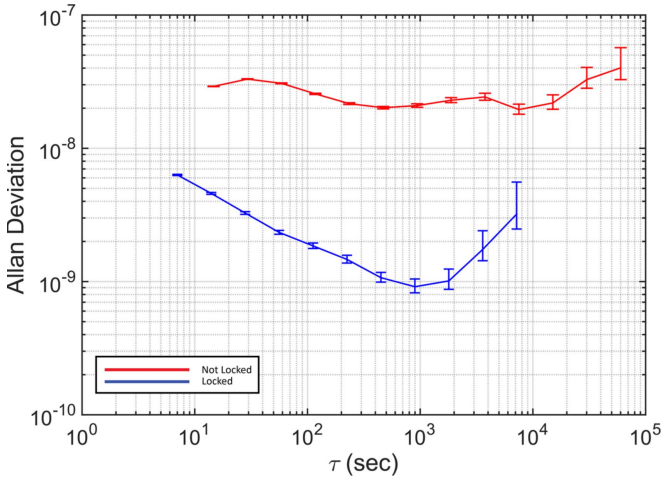

Figure 9. The Allan deviation of the beat between the L2 laser which is locked to the mm scale cell using FDROP and L3 laser which is locked to a reference cell using DROP (blue line). For comparison, we also plot the Allan deviation of the beat between the same two lasers, this time with locking (free running lasers).

The results are presented in figure 9. By observing the obtained Allan deviation, one can learn that we were able to stabilize a telecom band laser using our mm size cell to the level of 9×10^{-10} at around 1000 s (blue line). Such stability is more than an order of magnitude better than the stability of our free running laser.

6. Conclusions

In conclusion, we have introduced theoretically and demonstrated experimentally a new approach which we coin FDROP in the ladder-type atomic system. It is shown that the contrast of fluorescence detection of the probe beam in the FDROP approach is higher than the transmission detection of the probe beam in DROP approach. This property is of particular importance in miniaturized cells, where the optical path is reduced, which in turn results in a lower optical contrast. Indeed, we have extracted both DROP and FDROP spectra from a millimeter-sized cell and it was shown that under specific conditions of temperature and coupling power, the FDROP signal is easily observable, while the detection of the DROP signal is more challenging. Following this observation, we have measured both the FDROP and the DROP spectrum under different conditions of coupling powers. The results clearly indicated that the FDROP is superior in contrast with respect to the DROP. Taking advantage of this desired property, we have used the FDROP to stabilize the frequency of a laser to the hyperfine structure of the $5P_{3/2}$–$4D_{5/2}$ transition in a millimeter-size cell. By beating the stabilized laser to another stabilized laser, we obtained frequency instability floor of 9×10^{-10} at around 1000 s in terms of Allan deviation. Such sources which are stabilized to miniaturized cells may play an important building block in diverse fields ranging e.g. from communication to metrology.

Acknowledgments

We acknowledge Accubeat Ltd for providing the miniaturized vapor cell. The research was supported by the ERC grant LIVIN.

Appendix

The population of the levels is found using the rate equations:

$$\frac{dn_1}{dt} = \Gamma_0 \cdot n_1 + \gamma_{31} \cdot n_3 + \gamma_{41} \cdot n_4,$$

$$\frac{dn_2}{dt} = -(A_{25}\cdot\rho(\Delta_p,\nu)+\Gamma_0)n_2+\gamma_{32}\cdot n_3+\gamma_{42}\cdot n_4 + (A_{52}\cdot\rho(\Delta_p,\nu)+\gamma_{52})\cdot n_5,$$

$$\frac{dn_3}{dt} = -(\gamma_{31}+\gamma_{32}+\Gamma_0)\cdot n_3+\gamma_{63}\cdot n_6,$$

$$\frac{dn_4}{dt} = -(\gamma_{42}+\gamma_{41}+\Gamma_0)\cdot n_4+\gamma_{64}\cdot n_6+\gamma_{74}\cdot n_7,$$

$$\frac{dn_5}{dt} = A_{25}\cdot\rho(\Delta_p,\nu)-(\gamma_{52}+\Gamma_0+A_{52}\cdot\rho(\Delta_p,\nu)+A_{56}\cdot\rho_1(\Delta_c,\nu) + A_{57}\cdot\rho(\Delta_c,\nu)+A_{58}\cdot\rho(\Delta_c,\nu))\cdot n_5+(\gamma_{65}+A_{65}\cdot\rho(\Delta_c,\nu))\cdot n_6 + (\gamma_{75}+A_{75}\cdot\rho(\Delta_c,\nu))\cdot n_7+(\gamma_{85}+A_{85}\cdot\rho(\Delta_c,\nu))\cdot n_8,$$

$$\frac{dn_6}{dt} = A_{56}\cdot\rho(\Delta_c,\nu)\cdot n_5-(A_{65}\cdot\rho(\Delta_c,\nu)+\Gamma_0+\gamma_{65}+\gamma_{64}+\gamma_{63})\cdot n_6,$$

$$\frac{dn_7}{dt} = A_{57}\cdot\rho(\Delta_c,\nu)\cdot n_5-(\Gamma_0+\gamma_{75}+\gamma_{74}+A_{75}\cdot\rho(\Delta_c,\nu))\cdot n_7,$$

$$\frac{dn_8}{dt} = A_{58}\cdot\rho(\Delta_c,\nu)\cdot n_5-(\Gamma_0+\gamma_{85}+A_{85}\cdot\rho(\Delta_c,\nu))\cdot n_8,$$

where Δ_c, Δ_p are the coupling and pump detuning respectively. Γ_0 which is the transit time and for Gaussian laser beam with $1/e^2$ radius R passing through dilute gas of atoms with mean velocity u, given by [17]

$$\Gamma_0 = \frac{2u\sqrt{\ln 2}}{R}.$$

γ_{ik} is the factorial decay rate which depends upon the ratio of the Clebsch–Gordan coefficients according to

$$\gamma_{ik} = \frac{C_{ik}^2}{\sum_m C^2{}_{mk}}\Gamma_k,$$

where, m denotes the decay state channels and the summation is over all these channels.

The spontaneous decay rate from $5P_{3/2}$ to $5S_{1/2}$ state is:

$$\Gamma_{3,4,5} = 2\pi\times 6.06\ \text{MHz}.$$

The spontaneous decay rate from $4D_{5/2}$ to $5P_{3/2}$ state is:

$$\Gamma_{6,7,8} = 2\pi\times 1.97\ \text{MHz}.$$

A_{ik}—is the Einstein coefficient for the absorption and stimulated emission of a photon

$$A_{ik} = \frac{\pi e^2}{\epsilon_0\hbar^2 g_i}\mu_0^2\cdot C_{ik}^2 = \frac{g_k}{g_i}A_{ki},$$

where C_{ik} is the Clebsch–Gordan coefficients which can be calculated according to, e.g. [14, 18]. g_k, g_i denote the state degeneracy. $\rho(\Delta,\nu)$ is the normalized Lorentzian function, which characterizes the atom's response to the incident field

$$\rho(\Delta,\nu) = \frac{\frac{\gamma}{2\pi}}{(\Delta-k\cdot\nu)^2+\left(\frac{\gamma}{2}\right)^2},$$

where ω is the frequency of the laser, γ is the natural line width of the transition, k is the wave vector and ν is the velocity of the atom. We solve all the equations in the steady state condition:

$$\frac{dn}{dt} = 0.$$

After solving for the steady state condition, we sum over the excited states population and use it to calculate the intensity as a function of the detuning according to:

$$I_{flu}(\Delta)\propto\sum_{F'}\int_{-\infty}^{\infty}N_{F'}(\Delta,\nu)\cdot W(\nu)d\nu,$$

where F' is sum of all the excited states.

ORCID iDs

Eliran Talker https://orcid.org/0000-0001-7182-9762

References

[1] Fukuda K, Kinoshita M, Hasegawa A, Tachikawa M and Hosokawa M 2003 3–5 compact clocks using a thin cesium cell *J. Natl Inst. Inf. Commun. Technol.* **50** 95–104
[2] Knappe S, Shah V, Schwindt P D D, Hollberg L, Kitching J, Liew L A and Moreland J 2004 A microfabricated atomic clock *Appl. Phys. Lett.* **85** 1460–2
[3] Muller S T, Magalhaes D V, Alves R F and Bagnato V S 2011 Compact frequency standard based on an intra-cavity sample cold cesium atoms *J. Opt. Soc. Am.* B **28** 2592–6
[4] Dunning A, Gregory R, Bateman J, Himsworth M and Freegarde T 2015 Interferometric laser cooling of atomic rubidium *Phys. Rev. Lett.* **115** 1–5
[5] Cheng H D, Zhang W Z, Ma H Y, Liu L and Wang Y Z 2009 Laser cooling of rubidium atoms from background vapor in diffuse light *Phys. Rev.* A **79** 023407
[6] Demtröder W 2014 Basic Principles *Laser Spectroscopy 1* vol 1 (Berlin: Springer) (https://doi.org/10.1007/978-3-540-73418-5)
[7] Ludvigsen H, Äijälä A, Pietiläinen A, Talvitie H and Ikonen E 1994 Laser cooling of rubidium atoms in a vapor cell *Phys. Scr.* **49** 424–8
[8] Kominis I K, Kornack T W, Allred J C and Romalis M V 2003 A subfemtotesla multichannel atomic magnetometer *Nature* **422** 596–9
[9] Pustelny S 2015 Nonlinear magneto-optical rotation in rubidium vapor excited with blue light *Phys. Rev.* A **92** 053410
[10] Wickenbrock A, Leefer N, Blanchard J W, Budker D, Wickenbrock A, Leefer N, Blanchard J W and Budker D 2017 Eddy current imaging with an atomic radio-frequency magnetometer *Appl. Phys. Lett.* **108** 183507
[11] Weller L, Kleinbach K S, Zentile M A, Knappe S, Hughes I G and Adams C S 2012 Optical isolator using an atomic vapor in the hyperfine Paschen–Back regime *Opt. Lett.* **37** 3405
[12] Sasada H 1992 Wavenumber measurements of sub-Doppler spectral lines of Rb at 1.3 μm and 1.5 μm *IEEE Photonics Technol. Lett.* **4** 1307–9
[13] Moon H S, Lee L and Kim J B 2007 Double-resonance optical pumping of Rb atoms *J. Opt. Soc. Am.* B **24** 2157
[14] Siddons P, Adams C S, Ge C and Hughes I G 2008 Absolute absorption on the rubidium D lines: comparison between theory and experiment *J. Phys. B: At. Mol. Opt. Phys.* **41** 155004
[15] Breton M, Cyr N, Tremblay P, Têtu M and Boucher R 1993 Frequency locking of a 1324 nm DFB laser to an optically pumped rubidium vapor *IEEE Trans. Instrum. Meas.* **42** 162–6
[16] Moon H S, Lee W K, Lee L and Kim J B 2004 Double resonance optical pumping spectrum and its application for frequency stabilization of a laser diode *Appl. Phys. Lett.* **85** 3965–7
[17] Chebotayev P, Letokhov S, Lotsch M H K V, Schiifer F P, Queisser J, Wijn P J and Germany F R 1976 *Topics in Applied Physics* (vol 13) (Berlin: Springer)
[18] Steck D 2001 Rubidium 85 D line data Physics (College. Park. Md). 31